Annals of Science and Technology - A, Vol 6 (2): 28-46, 2021
Copyright: An Official *Journal* of the Nigerian Young Academy
ISSN: 2 544 6320

sciendo

ARTICLE

Phytoconstituents from *Markhamia Tomentosa* Bind To HPV Oncoprotein with Apoptogenic Potential: A Molecular Modeling Approach

Mutiat B. Ibrahim[1*], Adeola T. Kola-Mustapha[2], Niyi S. Adelakun[3] and Neil A. Koorbanally[4]

[1]Department of Pharmacognosy, Faculty of Pharmacy, University of Lagos, College of Medicine Campus, Idi-Araba, Lagos, Nigeria;
[2]Department of Pharmaceutics and Industrial Pharmacy, Faculty of Pharmaceutical Sciences, University of Ilorin, Nigeria;
[3]Chemogenomics Unit, Department of Biochemistry, Adekunle Ajasin University, Akungba-Akoko, Nigeria
[4]School of Chemistry and Physics, University of KwaZulu-Natal, Durban 4000, South Africa.

Received 31st August, 2021, Accepted 28th October, 2021
DOI: 10.2478/ast-2021-0008

**Corresponding author*
Mutiat B. Ibrahim E-mail: mutiat_ibrahim@yahoo.com; mibrahim@unilag.edu.ng
Tel: +234- 803 324 6915

Abstract

Markhamia tomentosa crude extract and fractions exhibited potent growth inhibitory effects capable to induce apoptosis in cervical (HeLa) cancer cell line via *in vitro* model. Presently, interaction of *M. tomentosa* phytoconstituents with molecular drug targets to exert its anticancer property is evaluated via *in silico* study. Identified phytoconstituents from *M. tomentosa* were retrieved from PubChem database and docked in active sites of HPV 16 E6, caspase -3 and caspase -8 targets using AutoDockVina from PyRx software. Screening for drug-likeness; and absorption, distribution, metabolism, excretion, and toxicity (ADMET) predictions was carried out with the use of SwissADME and pkCSM web servers. Standard melphalan and co-crystallized ligands of caspases -3 and -8 enzymes were used to validate protein-ligand interactions. Molecular dynamic simulation was used to validate the stability of the hit molecules complexed with caspases -3 and -8. All identified phytoconstituents from *M. tomentosa* showed binding affinity for HPV with docking scores range of - 5.4 to -2.6 kcal/mol. Ajugol, carnosol, luteolin and phytol showed good docking energy range of -6.8 to -3.6 kcal/mol; and -4.8 to -1.9 kcal/mol for the active sites of caspases -3 and -8 targets respectively. Based on docking scores; drug-likeliness; and ADMET predictions; luteolin and carnosol were selected as hit compounds. These molecules were found to be stable within the binding site of caspase -3 target throughout the 40ns simulation time. These findings identified hit ligands from *M. tomentosa* phytoconstituents that inhibit HPV 16 E6 oncogene expression with stimulation of caspases -3 and -8 targets.

Keywords: *Markhamia tomentosa*; HPV16 E6; Caspases; Molecular docking; Luteolin; Carnosol

BY-NC-ND *©2021 Ibrahim et al.* This work is licensed under the **Creative Commons Attribution-Non-Commercial-NoDerivs License 4.0**

1.0 Introduction

Human papilloma viruses (HPVs) have been identified as the primary etiological agent of cervical cancer. More so viral DNA from a specific group of the virus is detected in at least 90% of cervical cancer cases (Horvath et al., 2010; Okunade, 2020). HPVs that affect the genital tract are subdivided into low-risk and high-risk categories. Low-risk (LR) HPVs such as types 6 and 11 normally cause benign warts which rarely lead to cancer. While high-risk (HR) HPVs such as types 16, 18, 31 and 45 are linked to the development of high-grade lesions (cervical intraepithelial neoplasia) that can progress to cancer (Garnett and Duerksen-Hughes, 2006; Kumar et al., 2015). E6 and E7 encode proteins of LR and HR -HPVs are referred to oncoproteins. The E6 and E7 oncoproteins of HR-HPVs contribute majorly to malignant transformation by binding to p53 and retinoblastoma (Rb) tumor suppressors respectively (Munger and Howley, 2002; Thomsen et al., 2014). HPV16 E6 protein play a vital role in the pathophysiology of cervical cancer, which is ranked as the third most common type of cancer among women worldwide (Arbyn et al., 2018).

Controlled regulation of cell cycle and removal of undesirable cells referred to as programmed cell death has been recognized as a key strategy to promote the effective elimination of cancer cells (Chen et al., 2008; Carneiro and El-Deiry, 2020). Apoptosis programmed cell death is characterized by stereotypic structural changes regulated by the Bcl-2 family of proteins and executed by cysteine-aspartate proteases (caspases) (Allen et al., 1993; Wei et al., 2001; Deepa et al., 2019). Caspase family of cysteine protease enzymes has been an intensely studied target in drug design for many years (Ghavami et al., 2009; Shalini et al., 2015). Among the identified 14 mammalian caspases caspase -2, -3, -6, -7, -8, -9, and -10 were described as apoptotic caspases (Aly et al., 2020; El-Sheref et al., 2020). Apoptotic caspases are classified based on the site and mechanism of action as initiator caspases (caspase-2, -8, -9, -10) and executioner caspases (caspase-3, -6, -7). Caspase-8 mediates the extrinsic cell death pathway while caspase-3 mediates both extrinsic and intrinsic apoptotic pathways (Loison et al., 2014; Ashkenazi, 2015; Desai and Joshi, 2019). Molecular modeling approaches have been used in the development of HPV inhibitors with potential apoptogenic effect via involvement of caspases -3 and -8 (Senthil et al., 2011; Bucur et al., 2015; Desai and Joshi, 2019; Kashaw et al., 2019).

Although HPVs have been identified as causative agent for cervical cancer for more than three decades, the effective treatment against HPV infection is yet to be ascertained (Bharti et al., 2009; Kumar et al., 2015). Natural compounds obtained from plants have gained a significant interest among cancer researchers due to the potential to influence multiple cancer hallmarks (Mahomoodally 2013). Drugs derived from natural products with various biological activities such as antimicrobial, immune suppressive, anticoagulant and anticancer are capable to treat a significant number of categorized human diseases (Deepa et al., 2019). Therapeutic herbs therefore play an important role in the invention and generation of modern drugs that can be used in the treatment and management of cancer (Sagar et al., 2006; Gordaliza 2007; Yin et al., 2013).

Markhamia tomentosa (Benth.) K. Schum ex Engl. (Bignoniaceae) is a tree found mostly in West African countries including Senegal, Ghana, Nigeria, Cameroun, Congo and Angola. Different parts of the plant have been reported to exhibit anti-inflammatory, anti-oxidant, anti-ulcer, anti-microbial, anti-alzeheimer activities (Aladesanmi et al., 2007; Elufioye et al., 2010; Sowemimo et al., 2013; Sofidiya et al., 2014). Ibrahim et al. (2013) demonstrated anti-proliferative activity of *M. tomentosa* leaf extract through induction of intrinsic pathway of apoptosis evident by depolarization of the mitochondrial membrane of HeLa (cervical) cancer cells via *in vitro* study. More so antiproliferative compounds from the different solvent fractions of *M. tomentosa* crude extract had been identified and characterized (Ibrahim et al., 2018). However, the possible involvement of caspases in the apoptotic mechanism of cell viability inhibition of the plant extract and its constituents have not been established.

Therefore, in this study, the binding efficiency towards oncoprotein target through stimulation of caspase -3 and caspase -8 enzymes as well as pharmacokinetic analysis of phytoconstituents from the leaves of *M. tomentosa* are being evaluated via a molecular modeling approach.

2.0 Experimental

Identification of phytoconstituents from leaves of Markhamia tomentosa

Characterization of bioactive compounds from ethyl-acetate fraction of *M. tomentosa* crude leaf extract via electrospray ionization mass spectrometry were earlier reported by Sofidiya et al. (2014). Isolation and purification of biologically active compounds from ethyl-acetate and dichloromethane fractions of crude extract of leaves of *M. tomentosa* followed by identification through 1D and 2D NMR spectroscopic techniques were previously described by Ibrahim et al. (2018).

Retrieval of ligands

The SDF (Structure-data file) of identified phytoconstituents from *M. tomentosa*, standard melphalan and co-crystallized ligands were obtained from PubChem database (www.pubchem.ncbi.nlm.nih.gov/). The Pubchem CID of the ligands were retrieved from the database. Three-dimensional (3D) conformer of the retrieved chemical structure of the compounds were constructed in BIOVIA Discovery studio (Discovery Studio, Release 2020) visualization tool (BIOVIA 2020).

Retrieval and preparation of protein targets

The 3D conformer of the crystal structures of HPV 16 E6 oncoprotein (PDB ID – 4JOP); caspase -3 (PDB ID - 2XZT); and caspase -8 (PDB ID - 4PS1) enzymes were downloaded from the (http://www.rcsb.org) RCSB protein databank (Desai and Joshi 2019). The co-crystallized ligands and water molecules attached to the proteins were deleted prior to energy minimization process. The structures were converted to PDB file format and subjected to energy minimization by the steepest descent method using Chimera tool UCSF 1.14 at a conjugate gradient step of 0.02 Å (Pettersen et al., 2004). Hydrogen atoms were added as required, Gasteiger charges were assigned and the AMBER ff14SB force field was applied for energy minimization. The low energy

and stabilized conformations of the proteins were filed and saved as pdbqt file format for further studies.

Determination of active sites on protein

The amino acids present in the active sites of the proteins were determined using the Computed Atlas for Surface Topography of Proteins (CASTp) (http://sts.bioe.uic.edu/castp/index.html) server and Uniprot Knowledgebase (UniProtKB) protein database. Analyses of grid box dimensions and molecular docking evaluation were performed in the active sites of the proteins.

Molecular docking

Docking of ligands to target proteins and evaluation of the binding affinities were performed using AutoDockVina from PyRx (Dallakyan and Olson, 2015).

Drug-likeness evaluation and ADMET predictions of phytoconstituents

Drug-likeness properties of ligands were evaluated using Lipinski rule of five (RO5) and Vebers rule as calculated using SwissADME prediction (http://www.swissadme.ch/) server (Daina et al., 2017). Pharmacokinetic (absorption, distribution, metabolism and excretion) properties, as well as toxicity profile (ADME/T) of test, standard, and co-crystallized ligands were determined using an *in-silico* integrative model predicted at the pkCSM web server (Pires et al., 2015; Rowaiye et al., 2020).

Post-docking visualization and binding sites interaction

Molecular interactions between the top screened ligands with low binding energy, good drug-likeness and ADMET properties and protein targets were analysed for receptor-ligand interactions. The non-covalent interaction including the occurrence of hydrogen bond, van der Waals, pi-pi, pi-sigma, pi-sulfur and other hydrophobic interactions of the ligand-protein complex were viewed with Chimera tool UCSF 1.14 and BIOVIA Discovery studio 2020 (Bandyopadhyay et al., 2020; Johnson et al., 2020).

Molecular dynamics (MD) simulations

MD simulations of the Apo and Holo protein structures were performed using the Desmond software Maestro-Desmond Interoperability tools, 2018 (Bowers et al., 2006). Hit compounds from the phytoconstituents were identified and selected based on docking scores, drug-likeliness, and ADMET predictions. Briefly, the two hits with caspases -3 and -8 were prepared using the OPLS3 force field. The ligand-receptor docked complex was solvated in an orthorhombic box of TIP3P water model and 0.15 M NaCl was added into the system for sodium ion (Na^+) to neutralize the charges. The OPLS3 force field parameter was used in all simulations (Jorgensen et al., 1988; Harder et al., 2016). The system was relaxed by application of the default Desmond protocol (Bowers et al., 2006). The particle mesh Ewald (PME) method was employed to calculate the long-range part of the electrostatic interactions, while M-SHAKE algorithm was used for nonbonded interactions at 9 Å cut-off (Lambrakos et al., 1989; Darden et al., 1993). The simulation process was started with a primary energy minimization step using the steepest descent algorithm for 50,000 steps. The first two steps involved minimization with restraints on solute non-hydrogen atoms, then minimization without restraints using the Limited-memory Broyden-Fletcher-Goldfarb-Shanno (L-BFGS) algorithm with a convergence threshold of 1.0 kcal/mol/Å (Head and Zerner 1985). These steps were followed by equilibration through NVT and NPT ensembles using Berendsen dynamics with a coupling constant of 12 ps at 10 K with a 2.0 fs time step and restraints on the solute non-hydrogen atoms. The final steps of equilibration were by NPT ensemble using Berendsen dynamics at 300 K temperature, with and without restraints on the non-hydrogen atoms for 12 ps and 24 ps intervals respectively (Berendsen et al., 1984). Following the process of equilibration, 40 ns production run of the relaxed system was carried out using NPT ensemble with a Nose-Hoover thermostat and a Martyna-Tuckerman-Klein barostat at 300 K and 1.0 atm (Nosé 1984; Martyna et al., 1994). The simulation trajectories were computed using a multiple time step reversible reference system propagator algorithm (r-RESPA) integrator to solve the short-range bonded and long-range non-bonded interactions at 2.0 fs and 6.0 fs time steps respectively. Analysis of behavior and interactions between ligands and enzymes were performed using the Simulation Interaction Diagram (SID) tool implemented in Desmond MD package.

3.0 Results

Structure analysis of protein targets

Table 1 shows the experimental data and structure validation analysis including the sequence length of the target proteins and co-crystallized ligands. The 3D structures of HPV 16 E6 (PDB ID - 4JOP), caspase -3 (PDB ID - 2XZT), and caspase -8 (PDB ID - 4PS1) protein targets are as shown in Fig. 1.

Phytoconstituents from leaves of Markhamia tomentosa

Acteoside, luteolin, carnosol, dilapachone, tormentic acid, pomolic acid and ajugol compounds were identified in the ethyl-acetate fraction of *Markhmia tomentosa* via electrospray ionization mass spectrometry (Table 2). Sitosterol, cycloartenol, oleanolic acid and phytol compounds were isolated and characterized from dichloromethane and ethyl-acetate fractions of the crude leaf extract of *Markhamia tomentosa* (Table 2).

Retrieved ligands

2D structures of identified phytoconstituents: - acteoside, ajugol, carnosol, cycloartenol, dilapachone, luteolin, oleanolic acid, pomolic acid, phytol, sitosterol, and tormentic acid from *Markhamia tomentosa* are as shown in Fig. 2. The binding energies of test, standard and co-crystallized ligands to the active sites of the protein targets within the dimension of the grid box are as shown in Table 2.

Molecular docking

M. tomentosa phytoconstituents demonstrated varying degrees of binding affinities for the active sites of the oncogene and apoptotic targets as shown by the change in Gibb´s free energy (ΔG).

All identified phytoconstituents from *M. tomentosa* showed binding affinity for HPV 16 E6 oncogene protein target with binding energy value range of -5.4 kcal/mol to -2.6 kcal/mol (Table 2). Except for phytol (-2.6 kcal/mol) test ligand with lower docking score than

melphalan (-3.1 kcal/mol) standard ligand, all test ligands: dilapachone (-5.4 kcal/mol); carnosol (-4.3 kcal/mol); tormentic acid (-4.1 kcal/mol); acteoside, luteolin, and oleanolic acid (-4.0 kcal/mol); ajugol (-3.9 kcal/mol); pomolic acid and sitosterol (-3.8 kcal/mol) and cycloartenol (-3.6 kcal/mol) showed lower binding energy for HPV 16 oncogene protein (Table 2).

The binding energy of all test ligands for caspase -3 apoptotic target enzyme ranged from -6.8 kcal/mol to -3.6 kcal/mol. Luteolin (-6.8 kcal/mol); acteoside (-6.1 kcal/mol); pomolic acid (-6.0 kcal/mol); ajugol, oleanolic acid and tormentic acid (-5.9 kcal/mol); carnosol and cycloartenol (-5.7 kcal/mol), dilapachone (-5.5 kcal/mol); and sitosterol (-5.0 kcal/mol) test ligands with higher docking scores than melphalan (-4.3 kcal/mol) standard and MRD (-3.4 kcal/mol) co-crystallized ligands exhibited higher binding affinity for caspase -3 target (Table 2). Phytol also showed lower binding energy (-3.6 kcal/mol) against caspase -3 compared to its co-crystallized ligand.
The binding energy of interaction between test ligands of *M. tomentosa* and caspase -8 apoptotic target enzyme ranged from -4.8 kcal/mol to 48.3 kcal/mol (Table 2). Phytol (-4.8 kcal/mol) and luteolin (-3.7 kcal/mol) with lower binding energy than the co-crystallized (DTT) ligand (-3.2 kcal/mol) exhibited higher binding affinity for caspase -8 target. Except for ajugol (-2.4 kcal/mol) and carnosol (-1.9 kcal/mol) that also showed binding affinity for caspase -8, other test ligands from *M. tomentosa* showed no binding affinity for caspase -8 (Table 2).

Drug likeness behaviour of ligands

Table 3 shows the analysis of drug-likeness of test, standard and co-crystallized ligands using Lipinski rule of five (RO5) and Veber rule as well as molar refractivity property. Ajugol, carnosol, cycloartenol, luteolin, phytol, and sitosterol phytoconstituents with human bioavailability score of 0.55 passed the RO5 with zero to one violation (Table 3). Carnosol, cycloartenol, luteolin, and sitosterol test ligands passed the Veber rule with zero violation while ajugol, carnosol, luteolin, and phytol passed the molar refractivity property of drug-likeness with value range of 76.01 to 98.94 cm^3 (Table 3). Melphalan standard ligands and (MRD) and (DDT) co-crystalized ligands passed the Lipinski and Veber rules with zero violation and molar refractivity value range of 33.32 to 78.91 cm^3 (Table 3). Although dilapachone, oleanolic acid, pomolic acid, and tormentic acid passed the Lipinski and Veber rules with zero to one violation, these compounds did not pass the molar refractivity property of drug-likeness. As shown in table 3, acteoside test ligand with human bioavailability scores of 0.17 did not pass the RO5, Veber rule and molar refractivity property of drug-likeness.

ADMET property of ligands

The predicted values for absorption, distribution, metabolism, excretion, and toxicity of test, standard, and co-crystallized ligands are shown in Tables 4, 5, and 6. Acteoside, ajugol, carnosol, and luteolin test ligands are predicted to be substrates of P-glycoprotein while acteoside, carnosol, cycloartenol, dilapachone, phytol, and sitosterol test ligands are inhibitors of P-glycoprotein I and II (Table 4). Table 4 shows that cycloartenol, dilapachone, oleanolic acid, phytol, and sitosterol are predicted to be totally-bound to plasma protein. A log PS value greater than - 2 was predicted for carnosol, cycloartenol, oleanolic acid, pomolic acid, phytol, sitosterol, and tormentic acid test ligands.
As shown in Table 5, carnosol, cycloartenol, dilapachone, oleanolic acid, pomolic acid, phytol, sitosterol, and tormentic acid test ligands are predicted to be cytochrome CYP-3A4 substrates. Dilapachone, luteolin and phytol are predicted as inhibitors of CYP-2C9 and CYP-1A2 while carnosol and dilapachone are CYP-2C19 inhibitors. Dilapachone test ligand is also predicted as CYP-3A4 inhibitor (Table 5). As shown in Table 6, all test ligands from *M. tomentosa* as well as the standard and co-crystallized ligands are predicted as non-substrate of Renal Organic Cation Transporter 2 (OCT-2). Except for melphalan standard ligand, all test ligands from *M. tomentosa* and co-crystallized ligands of caspase -3 and caspase -8 enzymes are predicted to be non-mutagenic (Table 6). Standard, co-crystallized, and all test ligands except for oleanolic acid and pomolic acid are predicted to be non-hepatotoxic (Table 6).

Post-docking visualization and binding sites interaction

Hit ligands obtained from *M. tomentosa* phytoconstituents exhibited various non-covalent interactions with amino acid residues of the binding pockets of caspases -3 and -8 apoptotic target enzymes. Non-covalent interactions such as conventional hydrogen bond, carbon-hydrogen bond, van der Waals, pi-alkyl, pi-pi T shaped, pi-pi stacked, pi-sulfur, pi-sigma, pi-lone pair exist between the ligands and targets (Figs. 3 and 4). The interaction between carnosol with caspase -3 was strengthened by a conventional hydrogen bond with Arg 64 amino acid; carbon-hydrogen bond with His 121 and van der Waals interaction with Ser 65, Ser 120, Gly 122, Gln 161, Ala 162, Arg 164 amino acid residues (Fig. 3a). Luteolin interacted with the binding site of caspase -3 with six hydrogen bonds with Ser 63, Arg 64, Ser 65, Gly 122, Gln 161 and Gly 165 amino acid residues and van der Waals interaction with Thr 62, Thr 67, His 121, Ala 162 and Arg 164 residues (Fig. 3c). Similarly, melphalan standard ligand demonstrated hydrogen bond with Ser 65 amino acid residue along with van der Waals interaction with Gly 66, Thr 67, Ser 120, His 121, Gly 122, Gln 161, Gly 165 and Arg 164 amino acid residues (Fig. 3e). Figure 3b shows the 3D structure of carnosol within the binding pocket of caspase -3 with Leu 136, Thr 140, Phe 143, Arg 144, Lys 156, Ile 160 and Phe 168 amino acid side chains and hydrogen bond length range of 1.796 - 2.472 Å. Luteolin in the binding pocket of caspase -3 showed Thr 62, Ser 63, Arg 64, Ser 65, His 121, Gln 161 and Ala 162 amino acid side chains and hydrogen bond length range of 1.796 - 2.464 Å (Fig. 3d). The control standard ligand showed a bond length range of 1.802 – 2.298 Å with Arg 86, Lys 88, Leu 91, Thr 92, Glu 94, Ile 96, Glu 98, Leu 99, Asp 102 and Val 103 side-chain amino acid residues (Fig. 3f).

The His 317 and Cys 360 active site amino acid residues of caspase -8 formed van der Waals and hydrogen bond interactions respectively with carnosol and melphalan (Fig. 4a and 4e). While a pi-lone pair and a pi-sulfur interactions are seen with His 317 and Cys 360 amino acid residues and luteolin (Fig. 4c). Although Gly 318 and Tyr 324 formed an unfavorable donor-donor bond with carnosol, a pi-alkyl interaction along with van der Waals interaction with Leu 254, Ile 257, Asp 319, Asp 363, Val 410, Ser 411 and Arg 413 amino acid residues was formed with carnosol (Fig. 4a). Ser 316 and Asp 319 formed two hydrogen

 This journal is © The Nigerian Young Academy 2021

bonds with luteolin and the luteolin-caspase -8 complex was further strengthened by van der Waals interaction with Leu 254, Ile 257, Arg 260, Gly 318, Lys 320, Gln 358, Ala 359, Gly 362, Asp 363, Ser 411 and Arg 413 amino acid residues (Fig. 4c). Ile 333, Tyr 334, Glu 396, Ala 397, Phe 399, Leu 401 and Thr 469 amino acid side chains were seen with carnosol in the binding pocket of caspase -8 (Fig. 4b). Luteolin showed a bond length range of 2.128 - 2.238 Å with Arg 258, Tyr 412, Arg 413, Asn 414, Trp 420, and Asp 455 amino acid side chains within the binding pocket of caspase -8 (Fig. 4d). Fig. 4f shows melphalan standard ligand within the binding pocket of caspase -8 with Arg 260, Ser 316, His 317, Cys 360, Asp 363, Ser 411, Tyr 412, Arg 413 amino acid side chain residues and hydrogen bond length range of 2.055 - 2.566 Å.

Molecular dynamics (MD) simulation

A 40 ns long molecular dynamic simulations were performed for carnosol and luteolin and parameters such as root mean square deviation (RMSD), root mean square fluctuations (RMSF), and protein-ligand interactions for each protein-ligand complex were analyzed throughout the simulation trajectory.

Root mean square deviation (RMSD)

Fig. 5a– 5d shows RMSD values of the Cα atoms of caspase -3 apo state and caspase -3 complexed with carnosol, luteolin and melphalan standard ligands over 40 ns simulation run time. The RMSD Cα atom values for caspase -3 apo state are within 0.91 Å to 2.54 Å, while the average RMSD asymmetric carbon value is 1.49 Å (Fig. 5a). Carnosol-caspase -3 complex exhibited a RMSD Cα atom value range of 0.77 to 2.53Å with an average value of 1.48 Å throughout the 40 ns run time (Fig. 5b). Similarly, melphalan standard ligand complexed with caspase -3 showed RMSD Cα atom value range of 0.94 to 2.47 Å with an average value of 1.49 Å (Fig. 5d). Meanwhile the ligand-protein complex for luteolin with caspase -3 showed RMSD Cα atom value range of 0.81 to 2.68Å with an average value of 1.79 Å after 20 ns simulation run time (Fig. 5c).

The RMSD values of the Cα atoms for caspase -8 in carnosol, luteolin and melphalan standard ligands over 40 ns simulation run time are as shown in Fig. 6a–6d. The RMSD Cα atom values for apo state ranged within 1.11 Å to 6.96 Å with an average value of 5.56 Å (Fig. 6a). It was observed that the Cα atom of the ligand-protein complex for caspase -8 with luteolin showed a RMSD value range of 1.78 Å to 6.99 Å at an average of 5.94 Å throughout the 40 ns run time (Fig. 6c). The Cα atoms of caspase -8 complex with melphalan exhibited RMSD value range of 1.23 Å to 9.12 Å and carnosol showed range of 1.23 Å to 9.12 Å with average RMSD asymmetric carbon values of 6.60 Å and 7.24 Å respectively (Fig. 6b and 6d).

Root Mean Square Fluctuation (RMSF)

The RMSF values of the apo and ligand-protein complexes of carnosol and luteolin with caspase -3 are as shown in Fig. 7a–7d. It was shown that the alpha helices and beta strands of the apo structure and docked complexes oscillated within 0.30 Å to 0.78 Å. The loop regions of all the simulated systems showed large fluctuations up to 7.03 Å, 6.71 Å, 7.17 Å and 6.97 Å with a fluctuation average of 0.73 Å, 0.74 Å, 0.72 Å and 0.67 Å for the apo state, carnosol, luteolin and melphalan with caspase -3 target complexes respectively.

Fig. 8a- 8d shows the RMSF values of the Cα atoms for apo-caspase -8 and caspase -8 complex with carnosol, luteolin and melphalan. The alpha helices and beta strands of the apo structure and ligand-protein complexes oscillated within 0.40 Å to 1.56 Å. As shown in Fig. 8, loop regions of apo-caspase -8 and ligand-protein complex for caspase -8 with carnosol experienced large fluctuations up to 9.30 Å and 9.84 Å with a fluctuation average of 1.50 Å and 1.78 Å respectively. Meanwhile luteolin and melphalan- caspase 8 complexes displayed fluctuations up to 5.97 Å and 6.54 Å with a fluctuation average of 1.21 Å and 1.45 Å respectively.

Protein-ligand interactions

The protein-ligand interactions between amino acid residues of caspase-3 protein and carnosol, luteolin, and melphalan ligands across the simulation run time were computed and represented in Fig. 9a-9c. Carnosol, luteolin and melphalan shared hydrophobic interactions with amino acid residues Tyr 204 and Phe 256 that were sustained throughout the MD simulation. Except for Phe 256 amino acid that maintained minimal (below 20%) contact with melphalan, notable involvement of carnosol, luteolin and melphalan with Tyr 204 and Phe 256 amino acids was observed from 35% to 80% of the simulation run time. It was observed that carnosol and luteolin interacted with Thr 166 and Arg 207 amino acids mainly through hydrogen bond and H-bonding mediated by water bridge at less than 10% and 30% of the simulation run time (Fig. 9a and 9b). Conversely, H-bond, hydrophobic, ionic and H-bonding mediated by water bridges contacts were observed between carnosol and Arg 207 amino acid at about 30% and carnosol and melphalan with His 121, Glu 123 and Cso 163 amino acids from below 10% to about 100% of the simulation run time (Fig. 9a and 9c). Notably, melphalan exhibited H-bond interaction with Gly 122 amino acid at over 100% of the 40 ns simulation.

Furthermore, the interactions of all the ligands and individual amino acid residue in the binding pocket of caspase-8 was quantified and represented in Fig. 9dand 9f. Carnosol, luteolin and melphalan shared quite a few conserved interactions with Arg 258, His 317, Cys 360, Asp 363, Tyr 365, Val 410, and Arg 413 amino acid residues. As shown in the plot, luteolin and melphalan interacted with Arg 258 and Tyr 365 amino acids and carnosol alone interacted with Arg 413 amino acid via H-bond, hydrophobic, H-bonding facilitated by water bridges, and ionic contacts from 30% to 90% of the simulation run time (Fig. 9e and 9f). Carnosol made H-bond, hydrophobic, and H-bonding mediated by water bridges contacts at 10% and over 20% simulation run time with Arg 258 and Tyr 365 amino acids (Fig. 9d). Hydrophobic interactions with His 317 and Val 410 amino acid residues from about 10% to 40% of the simulation run time was also observed with all the ligands. The three ligands interacted with caspase-8 active site Cys 360 and Asp 363 amino acids mainly via H-bond, hydrophobic, and H-bonding mediated by water bridges contacts from 10% to 30% simulation run time. Carnosol and luteolin interacted with Ser 256, Ile 257, and Gly 362 amino acids mainly through H-bond, hydrophobic, and H-bonding mediated by water bridge at less than 10% and 30% of the simulation run time. H-bond, hydrophobic, H-bonding facilitated by water bridge, and ionic contacts with Ser 411, Tyr 412, Asp 455, Lys 457 and Asn 458

amino acid residues at about 10% simulation run time was seen with melphalan and carnosol (Fig. 9d and 9f). Notably, involvements of luteolin alone with Lys 253, Leu 254, Gly 318, Asp 319, Asn 364, and Tyr 324 amino acids via H-bond, hydrophobic, and H-bonding facilitated by water bridge contacts are observed from less than 10% to over 100% of the simulation time (Fig. 9e). While carnosol alone interacted minimally (below 10%) with amino acid residues Asn 414 and Pro 415 through H-bond, hydrophobic, and H-bonding facilitated by water bridge contacts (Fig. 9d).

Table 1: Structure analysis of HPV oncoprotein and caspases -3 and -8 apoptotic proteins

Experimental Data	HPV 16 E6 (4JOP)	Caspase -3 (2XZT)	Caspase -8 (4PS1)
Sequence length	7	149	275
Method	X-ray diffraction	X-ray diffraction	X-ray diffraction
Resolution	1.80 Å	2.70 Å	1.73 Å
Unit cell constants: Length (Å): a, b, c Angle (°): α, β, γ	a: 33.08Å, b: 48.40Å, c: 51.97Å; α: 90.00°, β: 101.00°, γ: 90.00°	a : 98.00Å, b: 98.00Å, c: 193.60Å; α: 90.00°, β: 90.00°, γ: 120.00°	a :115.87Å, b:144.60Å, c: 86.19Å; α: 90.00°, β: 123.86°, γ: 90.00°
R-Value Free	0.219	0.231	0.185
R-Value Work	0.179	0.197	0.152
R-Value Observed	0.181	0.199	0.154
Chains ID	C, D	A, C	A, B, C, D
Source of organism	Homo sapiens, Human papillomavirus type 16	Homo sapiens, synthetic construct	Homo sapiens
Co-crystallized ligand	-	(4R)-2-Methylpentane-2,4-diol (MRD)	2,3-Dihydroxy-1,4-dithiobutane (DTT)

Table 2: Docking energy of *M. tomentosa* phytoconstituents for HPV oncoprotein and caspases -3 and -8 apoptotic proteins and grid box parameters for active/binding sites docking

S/N	Ligands	PubChem CID	ΔG Energy (Kcal/mol) HPV 16 E6	Caspase -3	Caspase -8
1	Acteoside	5281800	-4.0	-6.1	6.2
2	Ajugol	6325127	-3.9	-5.9	-2.4
3	Carnosol	442009	-4.3	-5.7	-1.9
4	Cycloartenol	92110	-3.6	-5.7	21.7
5	Dilapachone	101733168	-5.4	-5.5	48.3
6	Luteolin	5280445	-4.0	-6.8	-3.7
7	Oleanolic acid	10494	-4.0	-5.9	30.8
8	Pomolic acid	382831	-3.8	-6.0	9.0
9	Phytol	5280435	-2.6	-3.6	-4.8
10	Sitosterol	22284	-3.8	-5.0	6.5
11	Tormentic acid	73193	-4.1	-5.9	18.2
12	Melphalan	460612	-3.1	-4.3	-4.3
13	(MRD)*	5288845	-2.3	-3.4	-3.5
14	(DDT)*	439196	-2.0	-3.3	-3.2
Grid box dimension					
Center X: Y: Z			30.55: 23.49: 24.76	22.23: -41.11: 9.57	-44.32: 23.08: 10.02
Size X: Y: Z:			17.62: 25.00: 12.71	15.77: 17.94: 12.71	15.77: 14.65: 12.71

*Co-crystallized ligands:
(MRD) - (4R)-2-methylpentane-2,4-diol for Caspase 3;
(DDT) - 2.3-dihydroxy-1,4-dithiobutane for caspase 8;

 This journal is © The Nigerian Young Academy 2021

Table 3: Drug-likeness of *M. tomentosa* phytoconstituents, standard and co-crystallized ligands

Compound	MW	ALog P	HBD	HBA	ROF violation	Human Oral Bioavalability	RB	PSA	Veber violation	Molar refractivity
Acteoside	624.59	-0.43	9	15	3	0.17	11	245.29	2	148.42
Ajugol	348.35	-1.76	6	9	1	0.55	3	149.07	1	77.67
Carnosol	330.42	3.72	2	4	0	0.55	1	66.76	0	92.83
Cycloartenol	426.72	7.15	1	1	1	0.55	4	20.23	0	135.14
Dilapachone	482.52	4.21	0	6	0	0.56	1	86.74	0	132.46
Luteolin	286.24	1.73	4	6	0	0.55	1	111.13	0	76.01
Oleanolic acid	456.7	6.06	2	3	1	0.85	1	57.53	0	136.65
Pomolic acid	472.7	5.13	3	4	1	0.56	1	77.76	0	138.11
Phytol	296.53	6.22	1	1	1	0.55	13	20.23	1	98.94
Sitosterol	414.71	7.19	1	1	1	0.55	6	20.23	0	133.23
Tormentic acid	488.7	4.33	4	5	0	0.56	1	97.99	0	139.28
Melphalan	305.2	1.32	2	3	0	0.55	8	66.56	0	78.91
(MRD)	118.17	0.69	2	2	0	0.55	2	40.46	0	33.32
(DDT)	154.25	0.04	2	2	0	0.55	3	118.06	0	39.52

MW: Molecular formular (< 500 Da): ALog P: Arithmetic log P (<5); HBD: Hydrogen bond donor (<5); HBA: Hydrogen bond acceptor (<10); ROF: Rule of five (Lipinski rule) violation; RB: Rotatable bond (<10); PSA: Polar surface area (<140 Å); Molar refractivity: (40 – 130 cm^3)

Table 4: *In-silico* absorption and distribution profile for test, known standard and co-crystallized ligands

Ligand	Human Intestinal Absorption (%)	P-gp substrate	P-gp I / II Inhibitor	Caco-2 permeability (log Papp in 10^{-6} cm/s)	BBBpermeability (Log BB)	CNS permeability (Log PS)	Fraction unbound in plasma
Acteoside	32.12	Substrate	Inhibitor / Non-inhibitor	0.10	- 1.86	- 4.60	0.27
Ajugol	31.80	Substrate	Non-inhibitor / Non-inhibitor	0.40	- 1.02	- 3.78	0.73
Carnosol	91.21	Substrate	Inhibitor / Non-inhibitor	0.57	- 0.10	- 1.82	0.04
Cycloartenol	95.25	Non-substrate	Inhibitor / Inhibitor	1.19	0.74	- 1.71	0.00
Dilapachone	100	Non-substrate	Inhibitor / Inhibitor	1.49	- 0.51	- 2.56	0.00
Luteolin	81.13	Substrate	Non-inhibitor / Non-inhibitor	0.10	- 0.91	- 2.25	0.17
Oleanolic acid	99.93	Non-substrate	Non-inhibitor / Non-inhibitor	1.17	- 0.14	- 1.16	0.00
Pomolic acid	97.97	Non-substrate	Non-inhibitor / Non-inhibitor	0.70	- 0.47	- 1.47	0.04
Phytol	90.71	Non-substrate	Non-inhibitor / Inhibitor	1.52	0.86	- 1.56	0.00
Sitosterol	94.46	Non-substrate	Inhibitor / Inhibitor	1.20	0.78	- 1.71	0.00
Tormentic acid	68.02	Non-Substrate	Non-inhibitor / Non-inhibitor	0.60	- 0.63	- 1.79	0.11
Melphalan	92.01	Substrate	Non-inhibitor / Non-inhibitor	0.85	- 0.07	- 2.93	0.44
(MRD)	85.07	Non-substrate	Non-inhibitor / Non-inhibitor	1.57	- 0.24	- 2.98	0.75
(DDT)	74.48	Non-substrate	Non-inhibitor / Non-inhibitor	1.54	- 0.28	- 3.20	0.77

Table 5: *In-silico* metabolism profile for standard and test ligands

Ligand	CYP-2C9 Substrate/Inhibitor	CYP-2D6 Substrate/Inhibitor	CYP-3A4 Substrate/Inhibitor	CYP-1A2 Inhibitor	CYP-2C19 Inhibitor
Acteoside	Non-substrate / Non-inhibitor	Non-substrate / Non-inhibitor	Non-substrate / Non-inhibitor	Non-inhibitor	Non-inhibitor
Ajugol	Non-substrate / Non-inhibitor	Non-substrate / Non-inhibitor	Non-substrate / Non-inhibitor	Non-inhibitor	Non-inhibitor
Carnosol	Non-substrate / Non-inhibitor	Non-substrate / Non-inhibitor	Substrate / Non-inhibitor	Non-inhibitor	Inhibitor
Cycloartenol	Non-substrate / Non-inhibitor	Non-substrate / Non-inhibitor	Substrate / Non-inhibitor	Non-inhibitor	Non-inhibitor
Dilapachone	Non-substrate / Non-inhibitor	Non-substrate / Non-inhibitor	Substrate / Inhibitor	Inhibitor	Inhibitor
Luteolin	Non-substrate / Inhibitor	Non-substrate / Non-inhibitor	Non-substrate / Non-inhibitor	Inhibitor	Non-inhibitor
Oleanolic acid	Non-substrate / Non-inhibitor	Non-substrate / Non-inhibitor	Substrate / Non-inhibitor	Non-inhibitor	Non-inhibitor
Pomolic acid	Non-substrate / Non-inhibitor	Non-substrate / Non-inhibitor	Substrate / Non-inhibitor	Non-inhibitor	Non-inhibitor
Phytol	Non-substrate / Inhibitor	Non-substrate / Non-inhibitor	Substrate / Non-inhibitor	Inhibitor	Non-inhibitor
Sitosterol	Non-substrate / Non-inhibitor	Non-substrate / Non-inhibitor	Substrate / Non-inhibitor	Non-inhibitor	Non-inhibitor
Tormentic acid	Non-substrate / Non-inhibitor	Non-substrate / Non-inhibitor	Substrate / Non-inhibitor	Non-inhibitor	Non-inhibitor
Melphalan	Non-substrate / Non-inhibitor	Non-substrate / Non-inhibitor	Non-substrate / Non-inhibitor	Non-inhibitor	Non-inhibitor
(MRD)	Non-substrate / Non-inhibitor	Non-substrate / Non-inhibitor	Non-substrate / Non-inhibitor	Non-inhibitor	Non-inhibitor
(DDT)	Non-substrate / Non-inhibitor	Non-substrate / Non-inhibitor	Non-substrate / Non-inhibitor	Non-inhibitor	Non-inhibitor

Table 6: *In-silico* excretion and toxicity profile for standard and test ligands

Ligand	Total clearance (log ml/min/kg)	Renal Organic Cation Transporter 2 (OCT2) substrate	Hepatotoxicity	Mutagenicity	Rat acute oral toxicity (LD_{50}; mol/kg)
Acteoside	0.48	No	No	No	2.53
Ajugol	1.23	No	No	No	2.70
Carnosol	0.28	No	No	No	2.19
Cycloartenol	0.26	No	No	No	2.63
Dilapachone	- 0.16	No	No	No	2.90
Luteolin	0.50	No	No	No	2.46
Oleanolic acid	- 0.08	No	Yes	No	2.35
Pomolic acid	0.08	No	Yes	No	2.32
Phytol	1.67	No	No	No	1.61
Sitosterol	0.63	No	No	No	2.55
Tormentic acid	0.09	No	No	No	2.42
Melphalan	0.63	No	No	Yes	2.48
(MRD)	0.75	No	No	No	1.61
(DDT)	0.59	No	No	No	1.69

 This journal is © The Nigerian Young Academy 2021

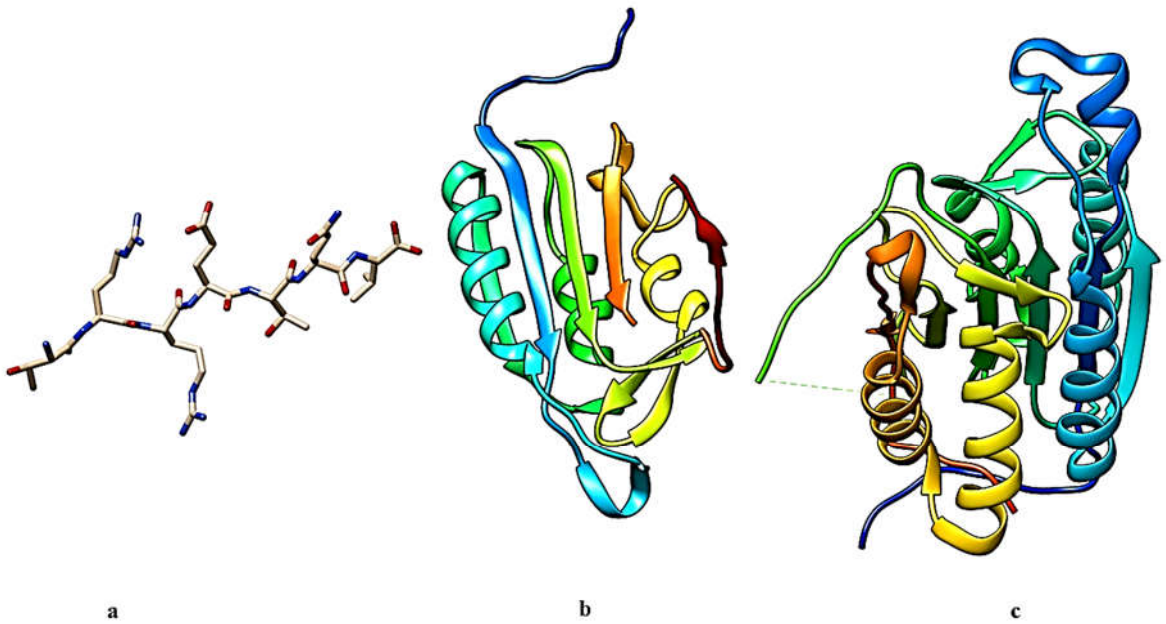


Fig. 1. 3D structures of **(a)** HPV 16 E6; **(b)** Caspase -3; **(c)** Caspase -8

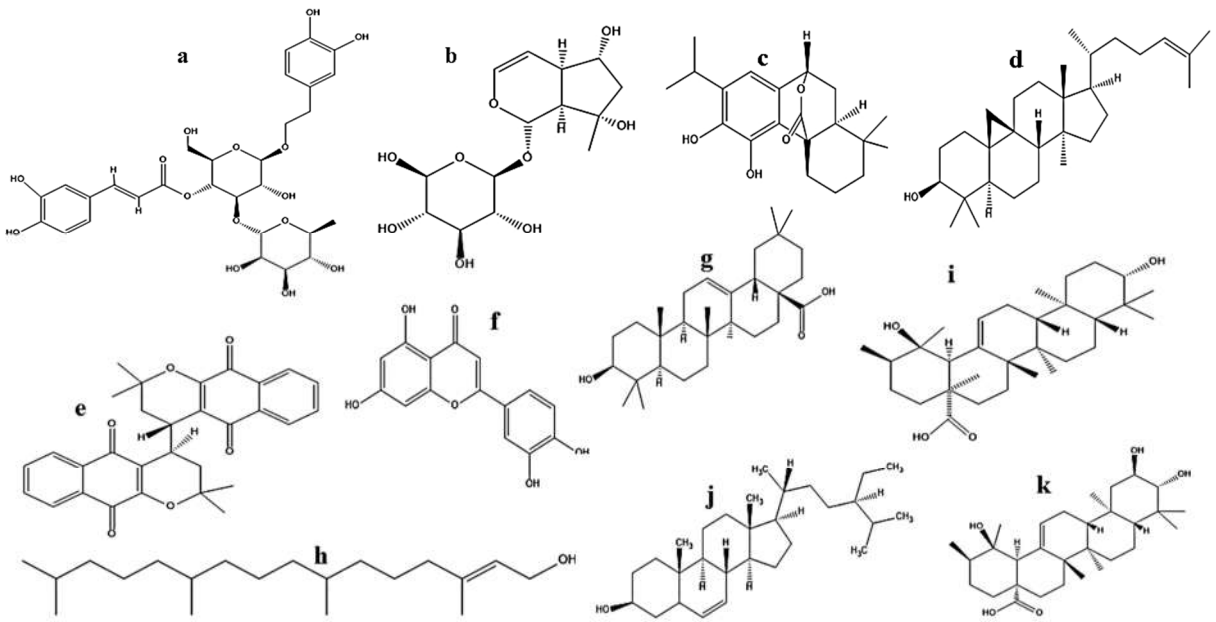


Fig. 2. 2D structures of **(a)** Acteoside **(b)** Ajugol **(c)**: Carnosol **(d)** Cycloartenol **(e)** Dilapachone **(f)** Luteolin **(g)** Oleanolic acid **(h)** Phytol **(i)** Pomolic acid **(j)** Sitosterol **(k)** Tormentic acid

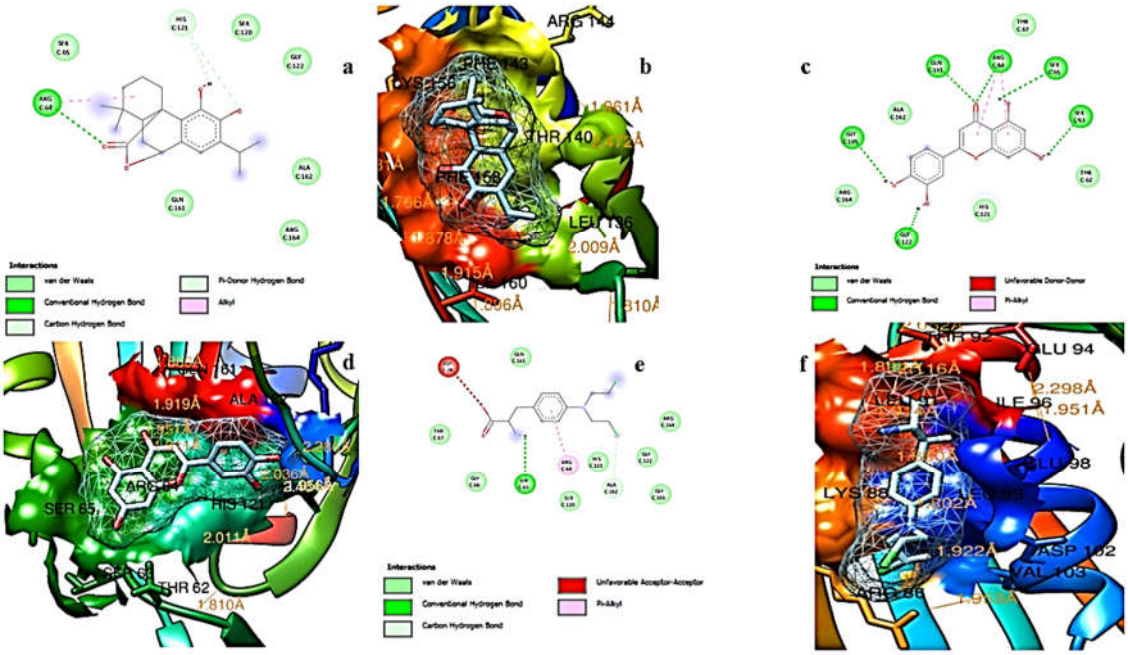


Fig. 3. 2D and 3D structures of **a** and **b**: Carnosol-caspase-3; **c** and **d**: Luteolin-caspase-3; **e** and **f**: Melphalan-caspase-3

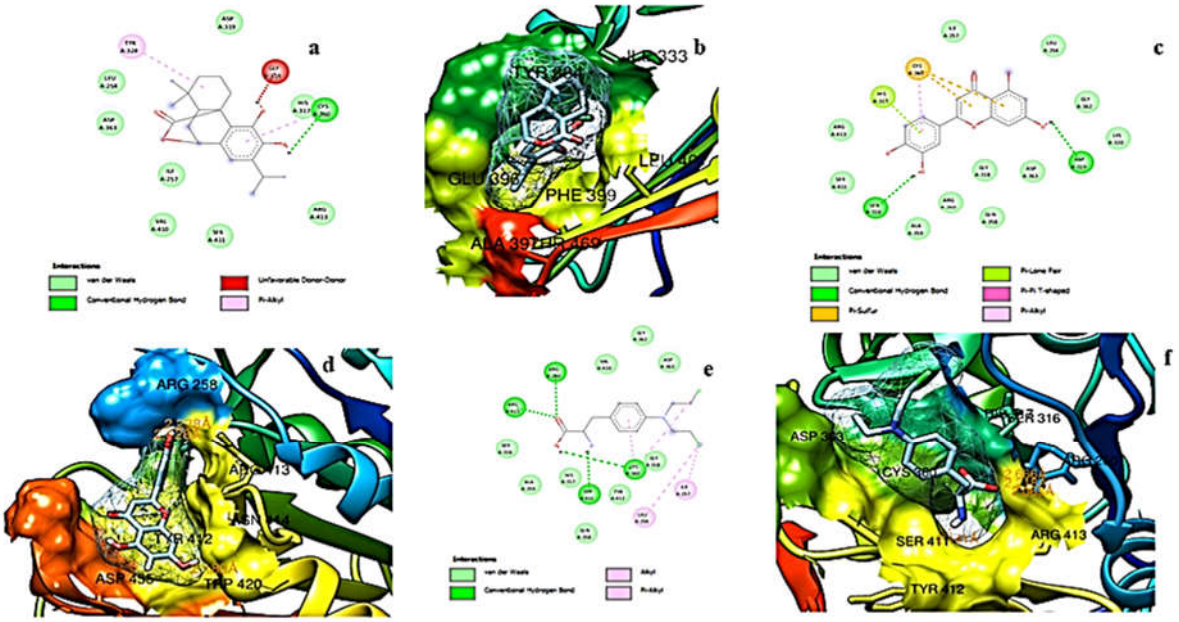


Fig. 4. 2D and 3D structures of **a** and **b**: Carnosol-caspase-8; **c** and **d**: Luteolin-caspase-8; **e** and **f**: Melphalan-caspase-8

 This journal is © The Nigerian Young Academy 2021

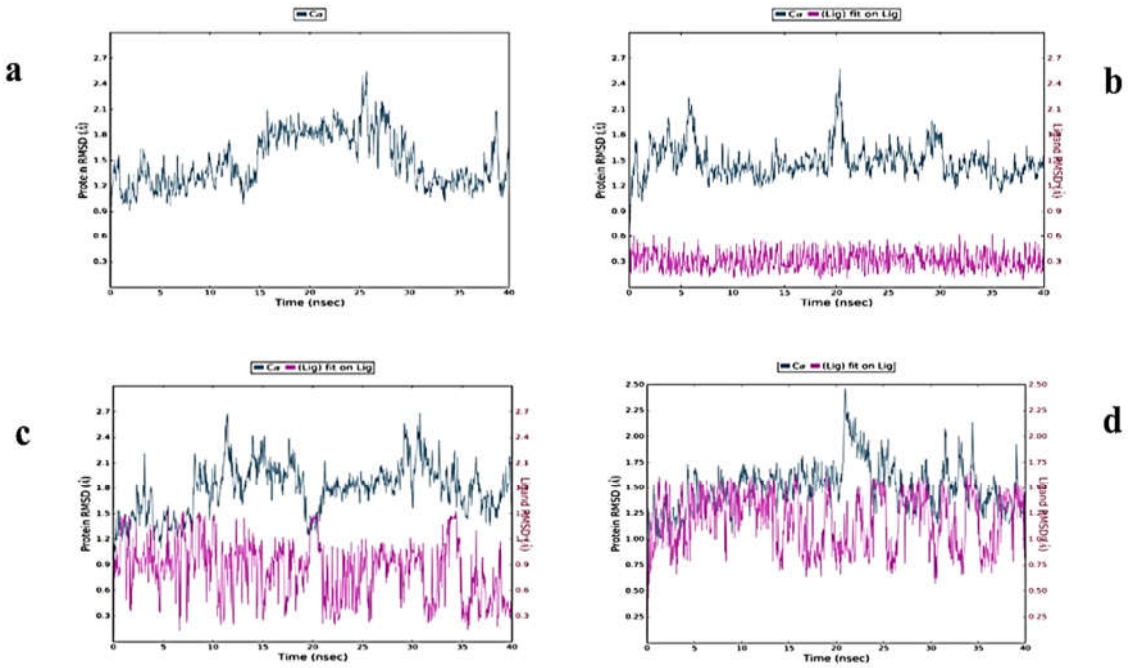


Fig. 5. RMSD of **a**: Apo-state of caspase -3; **b**: carnosol-caspase-3; **c**: luteolin-caspase-3; **d**: melphalan-caspase -3

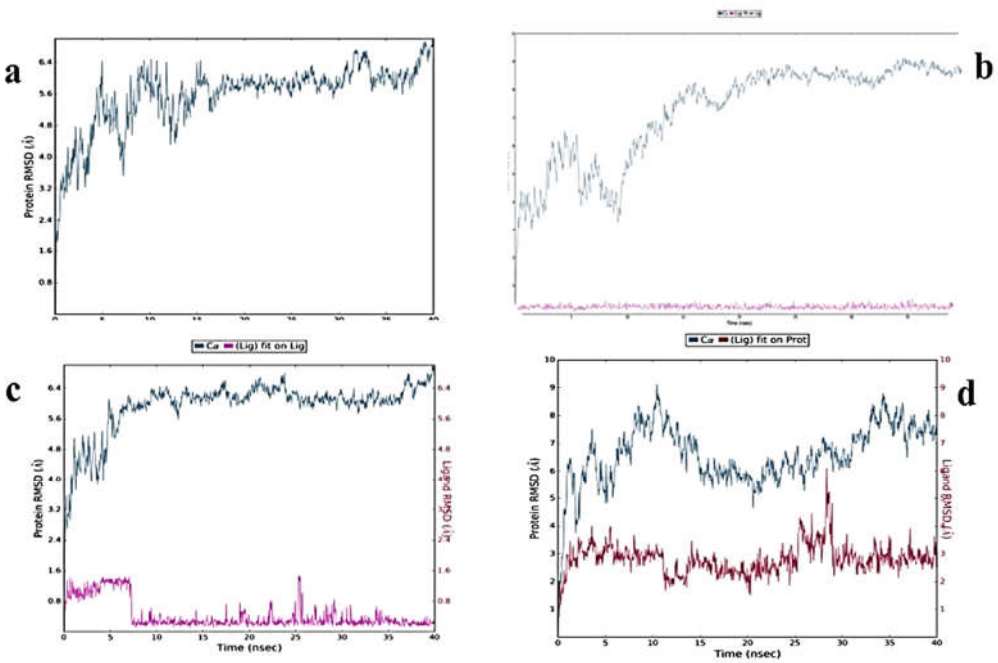


Fig. 6. RMSD of **a**: Apo-state of caspase -8; **b**: carnosol-caspase-8; **c**: luteolin-caspase-8; **d**: melphalan-caspase-8

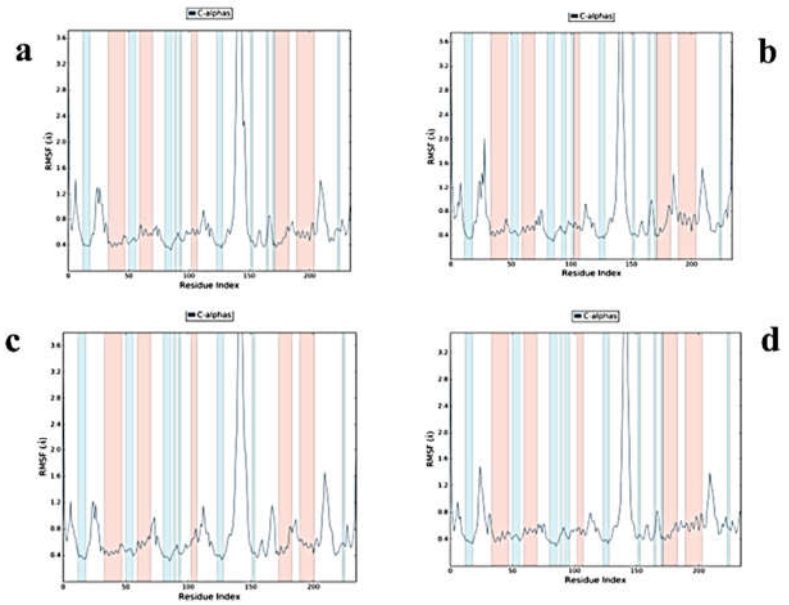


Fig. 7. RMSF of **a**: Apo-state of caspase -3; **b**: carnosol-caspase-3; **c**: luteolin-caspase-3; **d**: melphalan-caspase -3

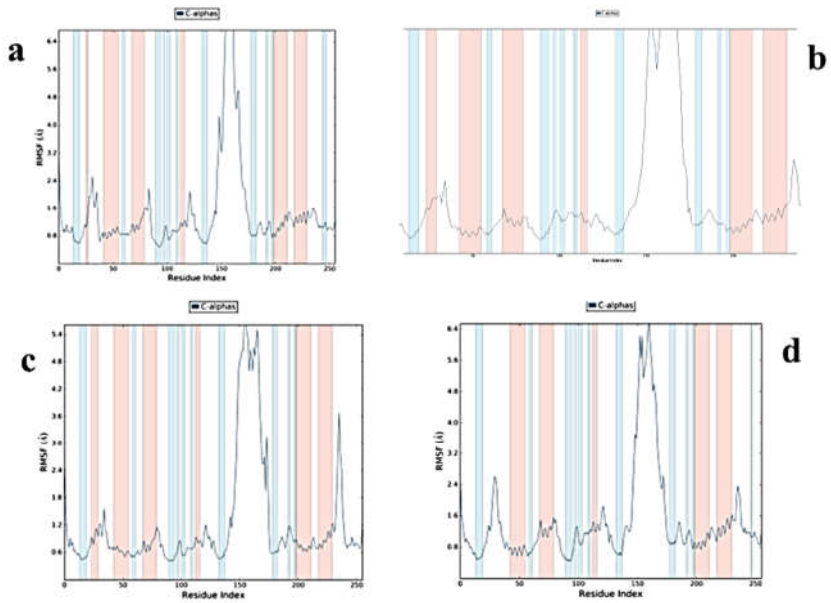


Fig. 8. RMSF of **a**: Apo-state of caspase -8; **b**: carnosol-caspase-8; **c**: luteolin-caspase-8; **d**: melphalan-caspase-8

 This journal is © The Nigerian Young Academy 2021

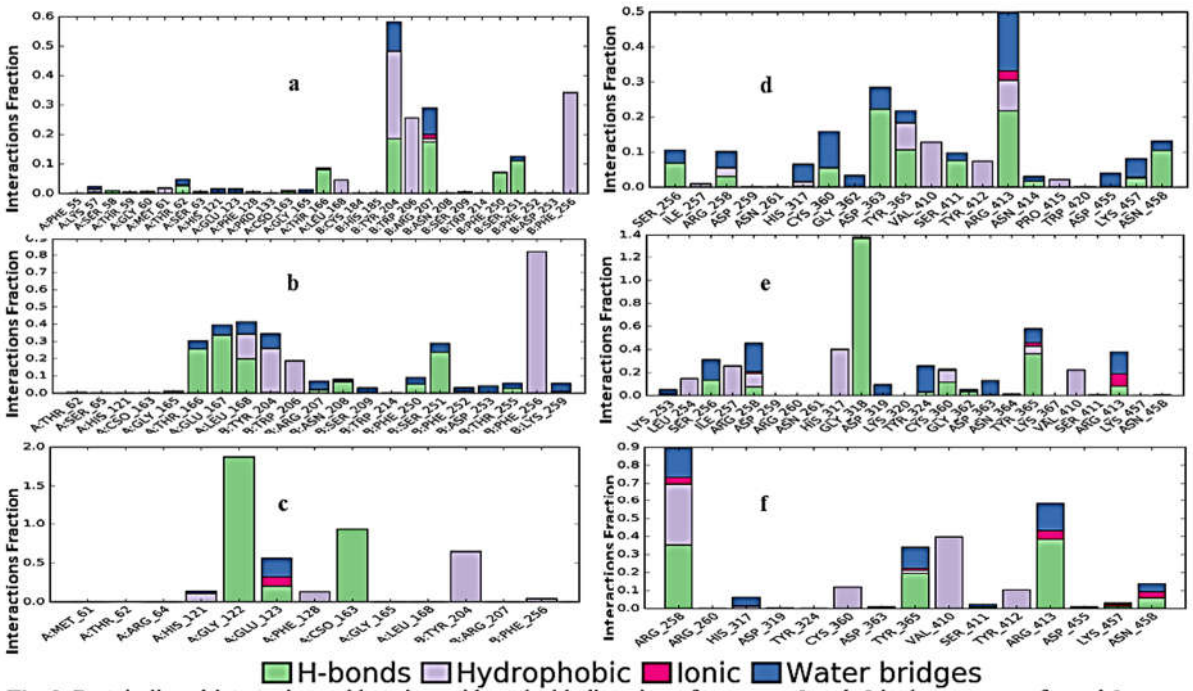


Fig. 9. Protein-ligand interactions with amino acids at the binding sites of caspases -3 and -8 in the presence of **a** and **d** – Carnosol; **b** and **e** – Luteolin; **c** and **f**: Melphalan

4.0 Discussion

Globally, cancer remains one of the major causes of death. Therefore, there is a need for continuous research towards the development of new, effective, and affordable anticancer drugs. Molecular docking, *in silico* ADME/T modeling, and molecular dynamic simulation serve as tools used in computational drug discovery for identification of lead compounds (Sehgal et al., 2016; Dali et al., 2019). The plant kingdom represents an enormous reservoir of bioactive phytochemicals, which are isolated and investigated for anticancer activity (Vital and Rivera, 2011). Medicinal plants with a long history of traditional usage but in the early stages of their pharmacological and phytochemistry studies are suitable for investigation via an *in-silico* approach to unveil their chemical mechanisms (Yi et al., 2018).

Markhamia tomentosa has found use in both human folk and ethnoveterinary medicines (Burkill 1985; Stark et al., 2013; Ibrahim et al., 2016). The antiproliferative and apoptosis-inducing capability of *M. tomentosa* leaf extract on cervical (HeLa) cancer cell line has been demonstrated (Ibrahim et al., 2013). Isolation and characterization of chemical constituents of *M. tomentosa* leaf extract revealed the presence of sitosterol, cycloartenol, phytol, oleanolic acid luteolin, ajugol, carnosol, pomolic acid, tormentic acid, dilapachone, and acteosidephyto-constituents (Sofidiya et al., 2014; Ibrahim et al., 2018).

In this present study, we carried out an *in-silico* analysis on phytoconstituents from *M. tomentosa* to predict the binding orientation towards oncogene and apoptotic enzyme targets. Drug-likeness and ADME/T properties of these phytochemicals were also predicted. Melphalan and co-crystallized ligands of target enzymes were used as control molecules to validate receptor-ligand interactions.

To the best of our knowledge, this is the first report describing the binding orientation of phytoconstituents from *Markhamia tomentosa* against oncogene and apoptotic enzyme targets. All tested phytoconstituents from *M. tomentosa* exhibited binding affinity for HPV 16 E6 oncoprotein and caspase -3 apoptotic enzyme. Similar to melphalan standard and MRD and DDT co-crystallized ligands, ajugol, carnosol, luteolin, and phytol test ligands from *M. tomentosa* showed a binding affinity with HPV oncogene and caspases -3 and -8 apoptotic enzyme targets. Similar *in-silico* study of phytochemicals from *Curcuma longa*, *Cosmos caudatus*, *Morinda lucida*, *Allium sativum*, *Aegle marmelos*, *Catharanthus roseus*, *Boerhaavia diffusa*, *Pseudarthira viscid*, *Pterocarpus marsupium*, and *Phyllanthus amarus* against apoptotic and anti-apoptotic protein targets have been reported in literature (Mala et al., 2015; Adewole and Ishola, 2019; Safitri et al., 2020). Luteolin, carnosol, phytol, sitosterol, cycloartenol, and acteoside have similarly been studied for induction of apoptotic cell death in cancer therapy via computational approach (Fu et al., 2012; Mustarichie et al., 2014; Ham et al., 2014; Yuan et al., 2016; Das et al.,

2018). Previous *in-vitro* study has also demonstrated that *M. tomentosa* extract inhibited cell viability and growth of cervical (HeLa) cancer cell through induction of intrinsic pathway of apoptosis (Ibrahim et al., 2013). It may be suggested from this result that ajugol, carnosol, luteolin and phytol phytoconstituents from *M. tomentosa* may inhibit expression of HPV 16 E6 oncogene via stimulation of caspase -3 or caspase -8.

Evaluation of the drug-likeliness property of bioactive chemical compounds is crucial in decision-making of prospective drug molecules to become an orally administered drug for human consumption. More so, early detection of problematic drug molecules improves the success rate of the process of drug discovery. Lipinski's rule of five (RO5) and Veber rule are used to evaluate the drug-likeliness property of drugs (Rowaiye et al., 2020). RO5 states that drugs with good oral bioavailability property must not violate more than one of the following criteria: molecular weight of less than 500 Daltons, octanol-water partition coefficient (log P) value of less than 5, less than or equals to 5 hydrogen bond donor and less than or equals to 10 hydrogen bonds acceptor (Lipinski et al., 2001). According to Veber rule, orally active drug should possess 10 or less rotable bonds and a topological polar surface area of less than 140 $Å^2$(Veber et al., 2002). Molar refractivity also indicates good oral bioavailability with value range of 40 - 130 cm^3 (Ghose et al., 1999). In this study, carnosol and luteolin compounds from *M. tomentosa* were in accordance with Lipinski and Veber rules as well as molar refractivity. More so both compounds ranked higher in binding affinity to oncoprotein and caspase -3 apoptotic enzyme targets than standard and co-crystallized ligands. Therefore, carnosol and luteolin phytoconstituents from *M. tomentosa* can be suggested as potential drug candidates.

Beyond efficacy, potential drug candidates should have good absorption, distribution, metabolism, excretion, and toxicity (ADMET) properties at a therapeutic dose (Guan et al., 2019). Absorption of drugs relies mainly on intestinal permeability and a drug molecule with human intestinal absorption (absorbance) value of less than 30% is considered to be poorly absorbed (Balimane et al., 2000; Pires et al., 2015; Lee et al., 2020). Carnosol and luteolin compounds from *M. tomentosa* exhibited good intestinal absorption similar to standard and co-crystallized ligands. Both compounds are predicted to be substrates of P-glycoprotein (P-gp), an indication that P-gp can recognize and cause efflux of these compounds. Thus, they should be co-administered with a P-gp inhibitor to facilitate their cellular absorption. The efficacy of a drug molecule may be affected by the extent to which it binds to plasma protein, as the more a drug is bound the less efficient it can diffuse (Pires et al., 2015). Luteolin and carnosol showed a similar proportion of free unbound drug with melphalan standard ligand but better distribution into human blood than other phytoconstituents of *M. tomentosa* that are totally bound to plasma protein. Cytochrome P450 (CYP-450) is an important detoxification enzyme that is involved in xenobiotic metabolism. Inhibition of an isoform of CYP-450 could cause cellular toxicity of its substrates (Nisha et al., 2016). Although CYP-450 inhibition profile for *M. tomentosa* phytoconstituents were assessed for five isoforms (CYP-2C9, CYP-2D6, CYP-3A4, CYP-1A2 and CYP-2C19), luteolin and carnosol hit compounds were predicted to be non-inhibitors of the two main isoforms (CYP-2D6 and CYP-3A4) responsible for drug metabolism (Pires et al., 2015). Furthermore, the hit compounds were inactive against renal excretion, hepatotoxicity, and mutagenicity parameters. Hence, carnosol and luteolin from *Markhamia tomentosa* are potential drug candidates with good ADME toxicity profile and can inhibit oncogene cell expression via involvement of caspases.

The interactions between carnosol and luteolin hit ligands and caspases -3 and -8 enzyme targets are a function of the amino acid residues at the active sites of the caspases. Caspases utilize a histidine-cysteine catalytic pair to hydrolyze peptide bonds after specific Aspartic acid residues (Stennicke and Salvasen, 1999; Clark, 2016). Hydrogen bonds formed between ligands and proteins play a vital role in the determination of the specificity and stability of the ligand-protein complex (Wade and Goodford, 1989; Steiner and Koellner, 2001; Weiss et al., 2001; Elekofihinti et al., 2018). The active site of caspase -3 (2XZT) contains histidine (His121) and cysteine (Cys163) amino acid residues with modification of cysteine residue to form S-nitrosocysteine (Cso163) residue. In this study, luteolin formed six hydrogen bonds with Ser 63, Arg 64, Ser 65, Gly 122, Gln 161 and Gly 165 amino acid residues of caspase -3 enzyme. Carnosol formed two hydrogen bonds with Arg 64 amino acid and His 121 active site amino acid residue of caspase -3 target enzyme. Similar to luteolin, melphalan standard ligand formed a hydrogen bond with Ser 65 amino acid residue. Caspase -8 (4PS1) contain histidine (His 317) and cysteine (Cys 360) amino acid residues at its active site. Carnosol, luteolin and melphalan formed one (Cys 360), two (Ser 316 and Asp 319), and four (Arg 260, Cys 360, Ser 411, and Arg 413) hydrogen bonds with amino acids of caspase -8 apoptotic enzyme target respectively. The Cys 360 active site amino acid residue of caspase -8 formed hydrogen bond with carnosol and melphalan. Similarly, previous studies have proven that caspases -3 and -8 docked with different types of compounds interacted with Asn 51, Ala 71, Arg 75, Asn 87, Asp 90, Asn 208, Gln 217, Leu 242, Ser 249, Asn 273 amino acids of caspase -3 and Asp 308, Glu 324, Thr 333, Asn 335, Gln 366, Gln 388, Thr 390, Thr 393 amino acids of caspase -8 (Govindarasu et al., 2017; Kashaw et al., 2018; Ismail et al., 2020; Safitri et al., 2020). The results herein indicate that protein-ligand interaction between caspases -3 and -8 enzymes and carnosol and luteolin hit ligands was strengthened by hydrogen bond with Ser 63, Arg 64, Ser 65, His 121, Gly 122, Gln 161 and Gly 165 amino acid residues of caspase -3 and Ser 316, Asp 319 and Cys 360 amino acid residues of caspase -8.

To further investigate the stability and flexibility of carnosol and luteolin complex with caspases -3 and -8 receptors, molecular dynamic MD simulations was performed. MD simulation is an important computational technique used to obtain binding mode information between ligands and receptors (Ge et al., 2013; Ahmad et al., 2020). Root mean square deviation (RMSD), root mean square fluctuation (RMSF) and protein-ligand contact parameters were analyzed during the simulation process. Analysis of RMSD and RMSF properties monitors the occurrence of possible abnormal structural changes over the simulation time (Lee et al., 2019; Adelakun et al., 2020). RMSD value < 2.0 Å corresponds to good docking solution; value between 2.0 and 3.0 Å deviate from the position of reference but with maintained desired orientation; and value > 3.0 Å is completely wrong (Gohlke et

 This journal is © The Nigerian Young Academy 2021

al. 2000; Mena-Ulecia et al. 2015; Ramirez and Caballero 2018). In this study, RMSD values for docked structures of carnosol and luteolin with caspase -3 were 1.48 Å and 1.79 Å and values with caspase -8 were 7.24 Å and 5.94 Å respectively. These results suggest that both carnosol and luteolin are stable in the binding site of caspase -3 during MD simulation with ΔG of -5.7 kcal/mol and -6.8 kcal/mol respectively. The instability of carnosol and luteolin in caspase -8 binding site with scoring average RMSD values of 7.24 Å and 5.94 Å was further translated into a poor binding free energy of -1.9 kcal/mol and -3.7 kcal/mol compared to carnosol and luteolin in caspase -3. RMSF is an expression of average residual mobility in a structure throughout the process of simulation and a higher RMSF value indicates more flexibility during MD simulation (Abouelelaet al. 2021). The result obtained from this study indicates that RMSF value for carnosol docked with caspase -3 is higher than with luteolin. Also, carnosol-caspase -8 complex showed a higher RMSF value than with luteolin. Protein-ligand contact is an important feature used in the analysis of the presence and absence of specific atomic-level interactions of ligand with binding site amino acids residues of proteins (Gandhimathi and Sowdhamini 2016; Lee et al. 2019). MD simulation aids to evaluate all the binding modes by averaging all protein-ligand contacts obtained from individual frames of the simulations and determines the most favorable interactions. Among the different amino acid residues that participated in the stability of luteolin-caspase -3 complex, major contribution was exhibited by Thr 166, Glu 167, Leu 168, Ser 251 amino acids in hydrogen bond interaction, Leu 168, Tyr 204, Trp 206, Phe 256 amino acids displayed hydrophobic interaction, Thr 166, Glu 167, Leu 168, Tyr 204, Ser 251 amino acids showed water bridges interaction without any observable ionic interaction. Hydrogen bond interaction with Tyr 204, Arg 207, Phe 250 and Ser 251 amino acids, hydrophobic interaction with Tyr 204, Trp 206 and Phe 256 residues, water bridges interaction with Tyr 204 and Arg 207 amino acids and ionic interaction with Arg 207 amino acid residue were the major contribution to the stability and flexibility of carnosol in the binding site of caspase -3. The protein-ligand intermolecular interactions confirm the stability and flexibility of carnosol and luteolin with the catalytic amino acid residues of caspase -3 throughout the MD simulations.

Conclusion

In this study, molecular docking was carried out to explore the binding interaction of *Markhamia tomentosa* phytoconstituents with HPV 16 E6 oncoprotein and caspase -3 and -8 enzymes. The correlation of the binding orientation with cell growth inhibitory activity of the phytoconstituents was also demonstrated. Following the docking of 11 natural compounds against oncogene and apoptotic targets and screening for drug-likeliness and good pharmacokinetic properties, two hit compounds were identified. Carnosol and luteolin hit compounds proved to be better drug candidates than standard and co-crystallized ligands in terms of bioavailability with optimal pharmacokinetic properties. Post docking analysis revealed that the hit ligands were involved in various non-covalent interactions within the active site cavity of the caspase -3 and -8 enzymes. Molecular dynamic simulations of 40 ns validated the stability of the carnosol-caspase-3 and luteolin-caspase-3 complexes. Although the results obtained from this *in silico* study is consistent with previous results from *in vitro* study which demonstrated inhibitory activity of extract of *M. tomentosa* against cervical (HeLa) cancer cell through induction of intrinsic pathway of apoptosis, further *in vivo* and *in vitro* studies on the phytoconstituents to validate this study are required.

Acknowledgements

The authors are grateful to the School of Chemistry and Physics, University of KwaZulu-Natal, South Africa where identification and elucidation of the phytoconstituents were carried out. Jaris Computational Center is acknowledged for providing the capacity building platform to acquire the skills of *in silico* analysis.

Declaration of Conflict of Interests

No conflict of interests.

Authors' Contributions

Conception: [ATK, MBI]
Design: [MBI, ATK, NSA, NAK]
Execution: [MBI, ATK, NSA, NAK]
Interpretation: [MBI, NSA]
Writing the paper: [MBI, ATK, NSA, NAK]

References

Abouelela, M.E., Assaf, H.K., Abdelhamid, R.A., Elkhyat, E.S., Sayed, A.M., Oszako, T., Belbahri, L., El Zowalaty, A.E., Abdelkader, M.S., 2021, Identification of potential SARS-CoV-2 main protease and spike protein inhibitors from the genus Aloe: An in-silico study for drug development. Molecules **26**: 1767. https://doi.org/10.3390/molecules26061767.

Adelakun, N., Obaseki, I., Adeniyi, A., Fapohunda, O., Obaseki, E., Omotuyi, O., 2020, Discovery of new promising USP14 inhibitors: computational evaluation of the thumb-palm pocket. Journal of Biomolecular Structure and Dynamics **10**: 1 - 11. doi: 10.1080/07391102.2020.1844803.

Adewole, K.E., Ishola, A.A., 2019, Phytosterols and triterpenes from MorindalucidaBenth (Rubiaceae) as potential inhibitors of anti-apoptotic BCL-XL, BCL-2, and MCL-1: an in-silico study. Journal of Receptor and Signal Transduction **39**(1): 87 - 97. doi.org/10.1080/10799893.20 19.1625062.

Ahmad, S.S., Sinha, M., Ahmad, K., Khaid, M., Choi, I., 2020, Study of caspase 8 inhibition for the management of Alzheimer's disease: A molecular docking and dynamics simulation. Molecules **25**: 2071. doi:10.3390/molecules25092071.

Aladesanmi, A.J., Iwalewa, E.O., Adebajo, A.C., Akinkunmi, E.O., Taiwo, B.J., Olorunmola, F.O., Lamikanra, A., 2007, Antimicrobial and antioxidant activities of some Nigerian medicinal plants. African Journal of Traditional and Complementary Alternative Medicine **4**: 173 - 184. doi: 10.4314/ajtcam.v4i2.31206.

Allen, P.D., Bustin, S.A., Newland, A.C., 1993, The role of apoptosis (programmed cell death) in haemopoiesis and the immune system. Blood Reviews **7**(1): 63 - 73.

Aly, A.A., Sayed, S.M., Abdelhafez, E.M., Abdelhafez, S.M.N., Abdelzaher, W.Y., Raslan, M.A., Ahmed, A.E., Thabet, K., El-Reedy, A.A.M., Brown,

A.B., Brase, S., 2020, New quinoline-2-one/pyrazole derivatives; design, synthesis, molecular docking, anti-apoptotic evaluation, and caspase-3 inhibition assay. Bioorganic Chemistry **94**: 103348.

Arbyn, M., Weiderpass, E., Bruni, L., de Sanjosé, S., Saraiya, M., Ferlay, J., Bray, F., 2020, Estimates of incidence and mortality of cervical cancer in 2018: a worldwide analysis. The Lancet Global Health **8**(2): E191-E203.

Ashkenazi, A., 2015, Targeting the extrinsic apoptotic pathway in cancer: Lessons learned and future directions. The Journal of Clinical Investigation **125**: 487 - 489.

Balimane, P.V., Chong, S., Morrison, R.A., 2000, Current methodologies used for evaluation of intestinal permeability and absorption. Journal of Pharmacology and Toxicological Methods **44**: 301 - 312. doi: 10.1016/S1056-8719(00)00113-1.

Bandyopadhyay, S., Abiodun, O.A., Ogboo, B.C., Kola-Mustapha, A.T., Attah, E.I., Edemhanria, L., Kumari, A., Jaganathan, R., Adelakun, N.S., 2020, Polypharmacology of some medicinal plant metabolites against SARS-CoV-2 and host targets: Molecular dynamics evaluation of NSP9 RNA binding protein. Theoretical and Computational Chemistry **1**: 1 - 40. doi:10.26434/chemrxiv.1294 5833.v1.

Berendsen, H.J.C., Postma, J.P.M., van Gunsteren, W.F., DiNola, A., Haak, J.R., 1984, Molecular dynamics with coupling to an external bath. Journal of Chemistry and Physics **81**: 3684 - 3690. doi:10.1063/1.448118.

Bharti,. A.C., Shukla, S., Mahata, S., Hedau, S., Das, B.C., 2009, Anti-human papillomavirus therapeutics: facts and future. The Indian Journal of Medical Research **130**: 296 - 310.

BIOVIA, DassaultSystèmes, Discovery stuidio, Release 2020, San Diego: DassaultSystèmes, 2020.

Bowers, K.J., Chow, D.E., Xu, H., Dror, R.O., Eastwood, M.P., Gregersen, B.A., Klepeis, J.L., Kolossvary, I., Moraes, M.A., Sacerdoti, F.D., Salmon, J.K., Shan, Y., Shaw, D.E., 2006, Scalable algorithms for molecular dynamics simulations on commodity clusters. SC '06: Proceedings of the 2006 ACM/IEEE Conference on Supercomputing 84. https://doi.org/10.1145/1188455.1188544.

Bucur, O., Gaidos, G., Yatawara, A., Pennarun, B., Rupasinghe, C., Roux, J., Andrei, S., Guo, B., Panaitiu, A., Pellegrini, M., Mierke, D.F., Khosravi-Far, R., 2015, A novel caspase 8 selective small molecule potentiates TRAIL induced cell death. Scientific Reports **5**: 9893. doi:10.1038/srep 09893.

Burkill, H.M., 1985, The Useful Plant of West Tropical African. Vol. 1. England: Royal Botanical Gardens, Kew 252 - 258.

Carneiro, B.A., El-Deiry, W.S., 2020, Targeting apoptosis in cancer therapy. Nature Reviews Clinical Oncology **17**: 395 - 417.

Chen, C.Y., Cheng, Y.B., Chen, S.Y., Chien, C.T., Kuo, Y.H., Guh, J.H., Khalil, A.T., Shen, Y.C., 2008, New bioactive clerodane diterpenoids from the roots of Casearia membranacea. Chemistry and Biodiversity **5**: 162 - 167.

Clark, C.A., 2016, Caspase allostery and conformational selection. Chemical Reviews **116**: 6666 – 6706. doi: 10.1021/acs.chemrev.5b00540.

Daina, A., Michielin, O., Zoete, V., 2017, SwissADME: A free web tool to evaluate pharmacokinetics, druglikeness and medicinal chemistry friendliness of small molecules. Scientific Reports **7**: 42717. doi:10.1038/srep42717.

Dali, Y., Abbasi, S.M., Khan, S.A.F., Larra, S.A., Rasool, R., Ain, Q.T., Jafar, T.H., 2019, Computational drug design and exploration of potent phytochemicals against cancer through in silico approaches. Biomedical Letters **5**(1): 21 - 26.

Dallakyan, S., Olson, A.J., 2015, Small-molecule library screening by docking with PyRx. Methods in Molecular Biology **1263**: 243 - 250.

Darden, T., York, D., Pedersen, L., 1993, Particle mesh Ewald: An N log(N) method for Ewald sums in large systems. The Journal of Chemistry and Physics **98**: 10089 - 10092. doi:10.1063/1063 /1.464397.

Das, S., Joardar, S., Manna, P., Dua, T.K., Bhattacharjee, N., Khanra, R., Bhowmick, S., Kalita, J., Saha, A., Ray, S., De Feo, V., Dewanjee, S., 2018, Carnosic Acid, a Natural Diterpene, Attenuates Arsenic-Induced Hepatotoxicity via Reducing Oxidative Stress, MAPK Activation, and Apoptotic Cell Death Pathway. Oxidative Medicine and Cellular Longevity **2018**: 1 - 24. doi. org/10.1155/2018/1421438.

Deepa, S.P., Harsh, G., Jha, A.K., 2019, Apoptosis caused by Natural compounds in cervical cancer cell line. Cancer Therapy and Oncology International Journal **14**(2): 555886. doi:10.19080/ CTOIJ.2019.14.555886.

Desai, T.H., Joshi, S.V., 2019, In silico evaluation of apoptogenic potential and toxicological profile of triterpenoids. Indian Journal of Pharmacology **51**(3): 181 - 207.

Elekofihinti, O.O., Ejelonu, O.C., Kamdem, J.P., Akinlosotu, O.B., Famuti, A., Adebowale, D.D., Iwaloye, O., Bulu, Y.I., Kade, I.J., Rocha, J.B.T., 2018, Discovery of potential visfactin activators using in silico docking and ADME predictions as therapy for type 2 diabetes. Beni-Suef University Journal of Basic and Applied Sciences **7**: 241 - 249.

El-Sheref, E.M., Aly, A.A., Alshammari, M.B., Brown, A.B., Abdel-Hafez, S.M.N., Abdelzaher, W.Y., Brase, S., Abdelhafez, E.M.N., 2020, Design, synthesis, molecular docking, antiapoptotic and caspase-3 inhibition of new 1,2,3-triazole/bis-2(1H)-Quinolinone hybrids. Molecules **25**: 5057. doi: 10.3390/molecules25215057.

Elufioye, T.O., Obuotor, E.M., Sennuga, A.T., Agbedahunsi, J.M., Adesanya, S.A., 2010, Acetylcholinesterase and butyrylcholinesterase inhibitory activity of some selected Nigerian medicinal plants. RevistaBrasileira de Farmacognosia**20**: 472 - 477.

Fu, J., Chen, D., Zhao, B., Zhao, Z., Zhou, J., Xu, Y., Xin, Y., Liu, C., Luo, L., Yin, Z., 2012, Luteolin induces carcinoma cell apoptosis through binding Hsp90 to suppress constitutive activation of STAT3. PLoS One **7**(11): e49194. doi: 10.1371/journal.pone.0049194.

Gandhimathi, A., Sowdhamini, R., 2016, Molecular modelling of human 5-hydroxytryptamine receptor (5-HT2A) and virtual screening studies

 This journal is © The Nigerian Young Academy 2021

towards the identification of agonist and antagonist molecules. Journal of Biomolecular Structure and Dynamics **34**: 952 -970.

Garnett, T.O., Duerksen-Hughes, P.J., 2006, Modulation of apoptosis by human papillomavirus (HPV) oncoproteins. Archives of Virology **151**(12): 2321 - 2335.

Ge, H., Wang, Y., Li, C., Chen, N., Xie, Y., Xu, M., He, Y., Gu, X., Wu, R., Gu, Q., Zeng, L., Xu, J., 2013, Molecular dynamics-based virtual screening: accelerating the drug discovery process by high-performance computing. Journal of Chemical Information and Modeling **53**: 2757 - 2764.

Ghavami, S., Hashemi, M., Ande, S.R., Yeganeh, B., Xiao, W., Eshraghi, M., Bus, C.J., Kadkhoda, K., Wiechec, E., Halayko, A.J., Los, M., 2009, Apoptosis and cancer: mutations within caspase genes. Journal of Medical Genetic **46**(8): 497 - 510. doi: 10.1136/jmg.2009.066944.

Ghose, A.K., Viswanadhan, V.N., Wendoloski, J.J., 1999, A knowledge-based approach in designing combinatorial or medicinal chemistry libraries for drug discovery. A qualitative and quantitative characterization of known drug databases. Journal of Combinatorial Chemistry **1**(1): 55 - 68. doi.org/10.1021/cc9800071.

Gohlke, H., Hendlich, M., Klebe, G., 2000, Knowledge-based scoring function to predict protein-ligand interactions. Journal of Molecular Biology **295**: 337 - 356. doi:10.1006/jmbi.1999.3371 PMID 10623530.

Gordaliza, M., 2007, Natural products as leads to anticancer drugs. Clinical and Translational Oncology **9**: 767 - 776.

Govindarasu, M., Palani, M., Vaiyapuri, M., 2017, In silico docking studies on Kaempferitrin with diverse inflammatory and apoptotic proteins functional approach towards the colon cancer. International Journal of Pharmacy and Pharmaceutical Sciences **9**(9): 199 - 204.

Guan, L., Hongbin, Y., Yingchun, C., Lixia, S., Peiwen, D.W.L., Guixia, L., Yun, T., 2019, ADMET-score – a comprehensive scoring function for evaluation of chemical drug-likeness. MedChemComm**10**(1): 148 – 157. doi: 10.1039/c8md00472b.

Ham, S., Kim, K.H., Kwon, T.H., Baki, Y., Lee, D.H., Song, Y.S., Park, S., Park, Y.S., Kim, M.S., Kang, J.W., Hong, J.T., Yoon, D., 2014, Luteolin induces intrinsic apoptosis via inhibition of E6/E7 oncogenes and activation of extrinsic and intrinsic signaling pathways in HPV-18-associated cells. Oncology Reports **31**: 2683 - 2691. doi: 10.3892/or.2014.3157.

Harder, E., Damm, W., Maple, J., Wu, C., Reboul, M., Xiang, J.Y., Wang, L., Lupyan, D., Dahlgren, M.K., Knight, J.L., Kaus, K.W., Cerutti, D.S., Krilov, G., Jorgensen, W.L., Abel, R., Friesner, R.A., 2016, OPLS3: A force field providing broad coverage of drug-like small molecules and proteins. Journal of Chemical Theory and Computation **12**: 281-296.

Head, J.D., Zerner, M.C., 1985, A Broyden-Fletcher-Goldfarb-Shanno optimization procedure for molecular geometrics. Chemical Physics Letters **122**: 264 - 270. doi:10.1016/0009-2614(85)80574-1.

Horvath, C.A.J., Boulet, G.A.V., Renoux, V.M., Delvenne, P.O., Bogers, J.J., 2010, Mechanisms of cell entry by human papillomaviruses: an overview. Virology Journal **7**(11): 1 - 7.

Ibrahim, B., Sowemimo, A., Spies, L., Koekomoer, T., van de Venter, M., Odukoya, O.A., 2013, Antiproliferative and apoptosis inducing activity of *Markhamia tomentosa* leaf extract on HeLa cells. Journal of Ethnopharmacology **149**: 745 - 749.

Ibrahim, M.B., Kaushik, N., Sowemimo, A.A., Odukoya, O.A., 2016, Review of the phytochemical and pharmacological studies of the genus *Markhamia*. Pharmacognosy Reviews **10**: 50 - 59.

Ibrahim, M.B., Sowemimo, A.A., Venables, L., Koorbanally, N.A., Awolola, G.V., Sofidiya, M.O., Odukoya, O.A., Koekemoer, T., van de Venter, M., 2018, Biological evaluation of phytoconstituents from *Markhamia tomentosa* ethanolic leaf extract. South African Journal of Botany **115**: 31 - 36.

Ismail, N.Z., Annamalai, N., Zain, N.N.M., Arsad, H., 2020, Molecular docking of selected compounds from *Clinacanthus nutans* with Bcl-2. P53, caspase -3 and caspase -8 proteins in the apoptotic pathway. Journal of Biological and Scientific Opinion **8**(1): 4 – 11. doi: 10.7897/2321-6328.081119.

Johnson, T.O., Odoh, K.D., Nwonuma, C.O., Akinsanmi, A.O., Adegboyega, A.E., 2020, Biochemical evaluation and molecular docking assessment of the anti-inflammatory potential of *Phyllanthus nivosus* leaf against ulcerative colitis. Heliyon **6**: e03893. doi.org/10.1016/j.heliyon. 2020.e03893.

Jorgensen, W.L., Tirado-Rives, J., 1988, The OPLS [optimized potentials for liquid simulations] potential functions for proteins, energy minimizations for crystals of cyclic peptides and crambin. Journal of the American Chemical Society **110**: 1657 - 1666.

Kashaw, S., Agarwal, S., Mishra, M., Sau, S., Iyer, A., 2019, Molecular docking analysis of caspase -3 activators as potential anticancer agents. Current Computer-Aided Drug Design **14**: 1. doi:10.2174/1573409914666181015150731

Kumar, S., Jena, L., Sahoo, M., Kakde, M., Daf, S,,Varma, A.K., 2015, In silico docking to explicate interface between plant-originated inhibitors and E6 oncogenic protein of highly threatening human papillomavirus 18. Genomics and Informatics **13**(2): 60 - 67. http://dx.doi.org/10.5808/Gl.2015.13.2.60.

Lambrakos, S.G., Boris, J.P., Oran, E.S., Chandrasekhar, I., Nagumo, M.A., 1989, A modified shake algorithm for maintaining rigid bonds in molecular dynamics simulations of large molecules. Journal of Computational Physics **85**: 473 – 486. doi: 10.1016/0021-9991(89)90160-5.

Lee, K.E., Bharadwaj, S., Yadava, U., Kang, S.G., 2019, Evaluation of caffeine as inhibitor against collagenase, elastase and tyrosinase using in silico and in vitro approach. Journal of Enzyme Inhibition and Medicinal Chemistry **34**(1): 927 - 936.

Lee, M., Ta, G.H., Weng, C., Leong, M.K., 2020, In Silico Prediction of Intestinal Permeability by Hierarchical Support Vector Regression. International Journal of Molecular Sciences **21**: 3582. doi:10.3390/ijms21103582.

Lipinski, C.A., Lombardo, F., Dominy, B.W., Feeney, P.J., 2001, Experimental and computational approaches to estimate solubility and permeability in drug discovery and development settings. Advanced Drug Delivery Reviews**46**: 3 - 26.

Loison, F., Zhu, H., Karatepe, K., Kasorn, A., Liu, P., Ye, K., Zhou, J., Cao, S., Gong, H., Jenne, D.E., Remol-O'Donnell, E., Xu, Y., Luo, H.R., 2014, Proteinase 3-dependent caspase-3 cleavage modulates neutrophil death and inflammation. The Journal of Clinical Investigation **124**: 4445 - 4458.

Mahomoodally, M.F., 2013, Traditional medicines in Africa: An appraisal of ten potent African medicinal plants. Evidence-based Complementary and Alternative Medicine **2013**: 1 - 14.

Mala, S.K., Priya, A.P., Bincy, B., Nazeem, P.A., 2015, Bioactive compounds to target anti apoptotic proteins- Bcl 2 and Bcl XL an in-silico approach. International Journal of Pharmaceutical Sciences and Research **6**(7): 3034 - 3043. doi: 10.13040/ijpsr.0975-8232.6(7).3034-43.

Martyna, G.J., Tobias, D.J., Klein, M.L., 1994, Constant pressure molecular dynamics algorithms. The Journal of Chemical Physics **101**: 4177 - 4189. doi:10.1063/1.467468.

Mena-Ulecia, K., Tiznado, W., Caballero, J., 2015, Study of the differential activity of thrombin inhibitors using docking, QSAR, molecular dynamics, and MM-GBSA. PLoS One **10**: e0142774.

Munger. K., Howley, P.M., 2002, Human papillomavirus immortalization and transformation functions. Virus Research **89**: 213 - 228.

Mustarichie, R., Levitas, J., Arpina, J., 2014, In silico study of curcumol, curcumenol, isocurcumenol, and β-sitosterol as potential inhibitors of estrogen receptor alpha of breast cancer. Medical Journal of Indonesia **23**(1): 15 - 24. doi.org/10.13181/mji.v23i1.684.

Nisha, C.M., Kumar, A., Vimal, A., Bai, B,M., Pal, D., Kumar, A., 2016, Docking and ADMET prediction of few GSK-3 inhibitors divulges 6-bromoindirubin-3-oxime as a potential inhibitor. Journal of Molecular Graphics and modelling **65**: 100 - 107. doi: 10.1016/j.jmgm.2016.03.001.

Nose, S.A., 1984, A unified formulation of the constant temperature molecular dynamics methods. The Journal of Chemical Physics **81**: 511 - 519. Doi:10.1063/1.447334.

Okunade, K.S., 2020. Human papillomavirus and cervical cancer. Journal of Obstetrics and Gynecology **40**(5): 602 - 608. doi:10.1080/01443615.2019.1634030.

Pettersen, E.F., Goddard, T.D., Huang, C.C., Couch, G.S., Greenblatt, D.M., Meng, E.C., Ferrin, T.E., 2004, UCSF Chimera—a visualization system for exploratory research and analysis. Journal of computational chemistry **25**(13): 1605 - 1612.

Pires, D.E.V., Blundell, T.L., Ascher, D.B., 2015, pkCSM: predicting small-molecule pharmacokinetic and toxicity properties using graph-based signatures. Journal of Medicinal Chemistry **58**(9): 4066 – 4072.

Ramirez, D., Caballero, J., 2018, Is it reliable to take the molecular docking top scoring position as the best solution without considering available structural data? Molecules **23**: 1038. doi:10.3390/molecules23051038.

Rowaiye, A.B., Onuh, O.A., Sunday, R.M., Abdulmalik, Z.D., Bur, D., Emeter, N.W., Obideyi, O.A., Pelletri, C.D., Ujah-Samuel, I.R., Iwuozor, C.R., Aondona, P.Y., Etalong, V.O., Yussuff, N., Akpa, J.N., 2020, Structure-based Virtual Screening and Molecular Dynamic Simulation Studies of the Natural Inhibitors of SARS-CoV-2 Main Protease. Journal of Ongoing Chemical Research **5**(1): 20 - 31. doi:10.5281/zenodo.3767102.

Safitri, A., Putri, A.S., Octavianty, T.D., Sari, D.R.T., 2020, Metabolomic profiles of *Curcuma longa* L and *Cosmos caudatus* extracts and their in-silico anti-cancer activity. Journal of Physics: Conference Series **1665**: 012022 doi:10.1088/1742-6596/1665/1/012022.

Sagar, S.M., Yance, D., Wong, R.K., 2006, Natural health products that inhibit angiogenesis: a potential source for investigational new agents to treat cancer: part 1. Current Oncology **13**: 14 - 26.

Sehgal, S.A., Mannan, S., Ali, S., 2016, Pharmacoinformatic and molecular docking studies reveal potential novel antidepressants against neurodegenerative disorders by targeting HSPB8. Drug Design, Development and Therapy **10**:1605.

Senthil, R.P., Ramya, R., Prakash, M., Pradhap, M., 2011, In silico docking analysis of marine derived compounds against oncoprotein of cervical cancer. International Journal of Recent Scientific Research **2**(4): 102 - 193.

Shalini, S., Dorstyn, L., Dawar, S, Kumar, S., 2015, Old, new and emerging functions of caspases. Cell Death Differentiation **22**(4): 526 - 539.

Sofidiya, M.O., Agunbiade, F.O., Koorbanally, N.A., Sowemimo, A., Soesan, D., Familusi, T., 2014, Antiulcer activity of the ethanolic extract and ethyl acetate fraction of the leaves of *Markhamia tomentosa* in rats. Journal of Ethnopharmacology **157**: 1 - 6.

Sowemimo, A., Samuel, F., Fageyinbo, M.S., 2013, Anti inflammatory activity of *Markhamia tomentosa* (Benth.) K. Schum. Ex Engl. ethanolic leaf extract. Journal of Ethnopharmacology **149**: 191 - 194.

Stark, T.D., Mtui, D.J., Balemba, O.B., 2013, Ethnopharmacological survey of plants use in the traditional treatment of gastrointestinal pain, inflammation and diarrhea in Africa: Future perspectives for integration in modern medicine. Animals **3**: 158 - 227.

Steiner, T., Koellner, G., 2001, Hydrogen bonds with pi-aceptors in proteins: Frequencies and role in stabilizing local 3D structures. Journal of Molecular Biology **305**: 535 - 557.

Stennicke, H.R., Salvesen, G.S., 1999, Catalytic Properties of the Caspases. Cell Death and Differentiation **6**: 1054 - 1059.

Thomsen, L.T., Frederiksen, K., Munk, C., Junge, J., Castle, P., Iftner, T., Kjaer, S.K.D., 2014, High-risk and low-risk human papillomavirus and the absolute risk of cervical intraepithelial neoplasia or cancer. Obstetrics and Gynecology **123**(1): 57 – 64.

Veber, D.F., Johnson, S.R., Cheng, H.Y., Smith, B.R., Ward, K.W., Kopple, K.D., 2002, Molecular properties that influence the oral bioavailability of drug candidates. Journal of Medicinal Chemistry **45**(12): 2615 - 2623. doi.org/10.1021/jm020017n.

Vital, P.G., Rivera, W.L., 2011, Antimicrobial activity, cytotoxicity, and phytochemical screening of *Voacanga globosa* (Blanco) Merr. Leaf extract. Asian Pacific Journal of Tropical Medicine **4** (10): 824 – 828.

 This journal is © The Nigerian Young Academy 2021

Wade, R.C., Goodford, P.J., 1989, The role of hydrogen-bonds in drug binding. Progress in Clinical and Biological Research **289**: 433 - 444.

Wei, M.C., Zong, W.X., Cheng, E.H., Lindsten, T., Panoutsakopoulou, V., Ross, A.J., Roth, K.A., MacGregor, G.R., Thompson, C.B., Korsmeyer, S.J., 2001, Proapoptotic BAX and BAK: a requisite gateway to mitochondrial dysfunction and death. Science **292**(5517): 727 - 730.

Weiss, M.S., Brandl, M., Suhnel, J., Pal, D., Hilgenfeld, R., 2001, More hydrogen bonds for the (structural) biologist. Trends in Biochemical Sciences **26**: 521 - 523.

Yi, F., Li, L., Xu, L., Meng, H., Dong, Y., Liu, H., Xiao, P., 2018, In silico approach in reveal traditional medicine plants pharmacological material basis. Chinese Medicine **13**(33): 1 - 20.

Yin, S.Y., Wei, W.C., Jian, F.Y., Yang, N.S., 2013, Therapeutic applications of herbal medicines for cancer patients. Evidence-Based Complementary and Alternative Medicine **2013**: 1 – 15 https://doi.org/10.1155/2013/302426.

Yuan, J., Ren, J., Wang, Y., He, X., Zhao, Y., 2016, Acteoside Binds to Caspase-3 and Exerts Neuroprotectionin the Rotenone Rat Model of Parkinson's Disease. PLoS One **11**(9): e0162696. doi: 10.1371/journal.pone.0162696.